Applied Catalysis B: Environmental 150–151 (2014) 515–522

Contents lists available at ScienceDirect

Applied Catalysis B: Environmental

journal homepage: www.elsevier.com/locate/apcatb

Yolk–shell structured Fe_3O_4@C@F-TiO_2 microspheres with surface fluorinated as recyclable visible-light driven photocatalysts

Guigao Liu[a,b], Fang He[a,b], Jing Zhang[a,b], Lijun Li[a,b], Fengjiao Li[a,b], Lixia Chen[a,b], Yuan Huang[a,b,*]

[a] School of Materials Science and Engineering, Tianjin University, Tianjin 300072, PR China
[b] Tianjin Key Laboratory of Composite and Functional Materials, Tianjin 300072, PR China

ARTICLE INFO

Article history:
Received 28 September 2013
Received in revised form
16 December 2013
Accepted 28 December 2013
Available online 8 January 2014

Keywords:
Yolk–shell structure
Surface fluorination
Magnetic microspheres
Visible-light
Photocatalytic activity

ABSTRACT

The uniform magnetic Fe_3O_4@C@fluorinated-TiO_2 (Fe_3O_4@C@F-TiO_2) microspheres with multilevel yolk–shell structures were successfully prepared by a simple and improved solvothermal method. The carbon mid-layer containing numerous hydrophilic groups induces TiO_2 growth onto its surface and plays a crucial role in protecting Fe_3O_4 cores from excessive erosion and keeping the integrity of the hollow structure during the solvothermal etching process, meanwhile as an electron acceptor it can reduce electron–hole recombination rate. In the presence of HF, the obtained TiO_2 shell possesses an enhanced crystallization resulting from the rapid *in situ* fluoride-mediated dissolution and recrystallization processes, and plenty of ≡Ti—F groups are formed on TiO_2 surface through the ligand replacement reaction between F^- and hydroxyl group. Furthermore, Fe_3O_4 cores will be partly etched by HF leading to the yolk–shell structure of an increased surface area of 167.50 m^2/g while Fe_3O_4@C@F-TiO_2 microspheres still maintain excellent magnetic separability. Due to the efficient molecular transportation and adsorption, and the synergic effect of carbon modification and surface fluorination of TiO_2, the Fe_3O_4@C@F-TiO_2 microspheres have been demonstrated to possess superior visible-light driven photocatalytic activity in degradation of Rhodamine-B than commercial P25 TiO_2 catalysts.

1. Introduction

Semiconductor photocatalysts are of pivotal importance for their potential application in environmental remediation and solar energy conversion [1]. Since Fujishima and Honda discovered photocatalytic water splitting on TiO_2 electrodes [2], TiO_2 has been intensively investigated due to its chemical inertness, strong oxidizing activity, long-term stability against photocorrosion and chemical corrosion, cost effectiveness, and nontoxicity [3]. However, the insufficient photocatalytic activity of TiO_2 catalyst under visible light still remains a major obstacle hindering its practical applications. Therefore, various strategies have been explored to improve its reactivity; such efforts include element (C, N, S, *etc.*) doping [4–6] and quantum dot (Ge [7], PbS [8], CdS [9], *etc.*) sensitizing to extend the optical absorption, optimization of the crystal structure to increase high-energy (0 0 1) facets exposing [10,11], and loading with noble metals to reduce recombination of photogenerated holes and electrons [12–15]. Among these approaches, F-doping or surface fluorination of TiO_2 attracts considerable attention [16,17]. After modified by fluorination, the surface acidity and polarity of TiO_2 can be significantly increased, which is greatly beneficial to adsorption of organic pollutant [3]. Furthermore, F-doping can improve the crystallinity and thermal stability of anatase and promote the production of mobile free OH radicals facilitating a better catalytic performance [16,17]. Therefore, the surface fluorination of TiO_2 has been regarded as one of most promising method to promote photocatalytic activity. However, aiming to improving the visible-light driven photocatalytic activity of TiO_2, the only efforts in the preparation of TiO_2 with surface fluorination are far from enough. In general, a high surface area is beneficial to a high adsorption of pollutants resulting in enhanced photocatalytic activity [18]. Therefore, an effective approach has been explored to improve the surface area of photocatalysts by building hollow structure [19–21]. Moreover, the hollow structure can endow catalysts many other advantages, like good surface permeability, and great light-harvesting capacity [22,23]. So far, a little success has been achieved to construct hollow TiO_2 with surface fluorination [21,22,24]. However, to the best of our knowledge, almost all existing preparation methods are based on fluoride-mediated self-transformation strategy whose process is difficult to control and the size of obtained hollow TiO_2 microspheres is excessively

* Corresponding author at: School of Materials Science and Engineering, Tianjin University, Tianjin 300072, PR China. Tel.: +86 15222017486.
E-mail address: yuanhuang@tju.edu.cn (Y. Huang).

0926-3373/$ – see front matter © 2014 Elsevier B.V. All rights reserved.
http://dx.doi.org/10.1016/j.apcatb.2013.12.050

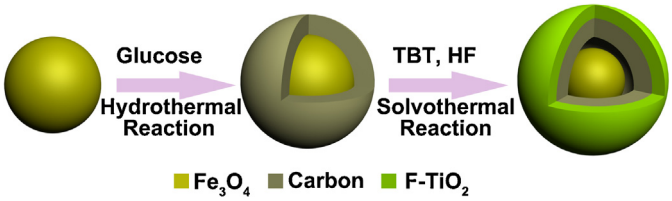

Scheme 1. Schematic illustration of the preparation process of the yolk–shell structured Fe_3O_4@C@F-TiO_2 microspheres.

large (>1 μm) and nonuniform leading to a limited surface area [21,23,24]. Therefore, it remains a great challenge to find a new strategy for preparation of hollow TiO_2 microspheres with surface fluorination, small size and high uniformity, which are expected to have a higher photocatalytic activity.

Currently, increasing attention is being focused on carbon based photocatalysts with enhanced photocatalytic activities [25]. The utilization of carbon in the composites of photocatalysts not only improves the separation of photogenerated electron–hole pairs due to its high electronic conductivity but also facilitates the concentration of pollutant molecules at the carbon/catalyst interface [25]. Hou et al. reported that the carbon modified $Bi_{12}TiO_{20}$ showed an excellent photocatalytic activity for degradation of Rhodamine-B ascribing to the reduced recombination of photogenerated electron–hole pairs associated with the carbon [26]. Li et al. prepared the P25-graphene composite showing a significant enhancement in photodegradation of methylene blue due to enhanced charge separation and transportation [27]. Although some carbon-modified TiO_2 with high photocatalytic activity have been reported, the investigation of TiO_2 modified by both carbon and surface fluorination is still open [25].

On the other hand, although TiO_2 has been proved to be an ideal candidate for treatment of water pollution, the efficient separation and recycling of this finely powdered catalyst is still a scientific problem when applied in practice. Thus a facile and effective approach to recover suspended TiO_2 particles is highly desirable. Fortunately, magnetic separation provides a suitable solution to this issue. By immobilized on various magnetic supports (such as carbon [28], silica [29], and polymer [30]) to form hybrid materials, TiO_2 catalyst can not only be collected with an external magnetic field but also inherit from the supports excellent surface chemistry, high mechanical properties, and good thermal stability [31]. As a result, successful strategies for preparation of magnetic TiO_2 hybrid catalysts are recognized as one of major advances in nanotechnology.

Herein, we carefully designed and synthesized a Fe_3O_4@C@fluorinated-TiO_2 (Fe_3O_4@C@F-TiO_2) yolk–shell structured catalyst which well addressed both the catalytic activity and recovery issues for photocatalysts. The preparation procedure of this catalyst is shown in Scheme 1. Fe_3O_4 particles were first synthesized as described previously [31], and then over-coated with a layer of amorphous carbon by hydrothermal reaction of glucose to obtain core–shell microspheres (denoted as Fe_3O_4@C). Finally, in the presence of hydrofluoric acid (HF), the Fe_3O_4@C microspheres were further coated with TiO_2 through hydrolyzing tetrabutyl orthotitanate (TBT) under solvothermal conditions. Through this elaborately designed procedure, the Fe_3O_4@C@F-TiO_2 yolk–shell microspheres, with small and uniform particle size, high surface area, excellent magnetic separability and, especially, the synergic effect of carbon modification and surface fluorination for TiO_2, were firstly prepared. It is noteworthy that the HF used here is not only as an additive to promote the growth of surface fluorinated anatase but also as an etching agent to partly etch Fe_3O_4 core resulting in the formation of carbon-supporting yolk–shell structure. Furthermore, the carbon mid-layer introduced is believed to also have three roles here: to induce the completely coating of TiO_2, to prevent the hollow structure from collapsing and to modify the TiO_2 shell as the electron acceptor and transporter. As expected, this kind of magnetic catalyst showed powerful visible-light catalytic activity in recyclable decomposition of Rhodamine-B (RhB).

2. Experimental

2.1. Preparation of Fe_3O_4 particles

All chemicals used were of analytical grade and purchased from Chinese domestic suppliers. The preparation of Fe_3O_4 particles was conducted according to the previous report with some modification [31]. Typically, $FeCl_3{\cdot}6H_2O$ (0.3 g) was dissolved in 9 ml of ethylene glycol to form a clear solution into which 1,6-hexanediamine (1.8 g) and anhydrous sodium acetate (0.6 g) were added. This mixture solution was stirred vigorously at 50 °C for 30 min and then transferred into a Teflon-lined autoclave and heated to 200 °C for 6 h. After cooling to room temperature, the Fe_3O_4 particles were collected and washed with water and ethanol for three times, and vacuum dried at 60 °C for 6 h.

2.2. Preparation of Fe_3O_4@C particles

20 mg of Fe_3O_4 particles were ultrasonicated for 5 min in a 0.1 M HNO_3 solution (20 ml), followed by washed several times in deionized water. Then the as-treated particles were redispersed in a 48 ml of 0.5 M aqueous glucose solution and the suspension was sealed in a Teflon-line autoclave (60 ml). The autoclave was kept at 180 °C for 4 h before cooling naturally. The products were separated and washed in water and ethanol and finally dried at 60 °C for 6 h.

2.3. Preparation of yolk–shell structured Fe_3O_4@C@F-TiO_2 particles

15 mg of Fe_3O_4@C particles were dispersed in absolute ethanol (40 ml) after ultrasonicating over 15 min. Subsequently, to this suspension, 48 μl of hydrofluoric acid solution (40 wt.%) and 0.4 ml of tetrabutyl orthotitanate (TBT) were added. This mixture was ultrasonicated for 10 min and transferred to a 60 ml Teflon-line autoclave which was then heated to 180 °C for 24 h. After the autoclave cooled down to room temperature, the products were collected (by a magnet), washed, and dried for further characterization.

2.4. Characterization

X-ray diffraction (XRD) was conducted on a Bruker D8 advance X-ray diffractometer at a scanning rate of 8°/min. Field-emission scanning electron microscopy (FESEM) was performed on a Hitachi S-4800 microscope. The morphology of products was determined by using an FEI Technai G2 F20 TEM and JEOL100 TEM. Their elemental composition was analyzed with an EDAX Genesis XM2 attached to the G2 F20 TEM. Chemical bonding information for sample was studied with a Nicolet 470 Fourier transform infrared (FTIR) spectrometer. UV–vis absorption spectra were recorded using a TU1810PC spectrophotometer (Beijing Purkinje General Instrument Co.). N_2 adsorption–desorption experiments were carried out at 77 K to examine the Brunauer–Emmett–Teller surface area and micropore volume (BJH method). Before measuring, the samples were degassed in a vacuum at 100 °C for 6 h. Magnetic measurements were performed with a superconducting quantum interference device (SQUID) magnetometer (Quantum Design PPMS-7). The thermal analysis was carried out with a Perkin Elmer

Diamond TG/DTA thermal analyzer up to 900 °C at a heating rate of 10 °C/min in air. X-ray photoelectron spectroscopy (XPS; PHI 5000 Versa-Probe) analysis was conducted using monochromatized Al Kα radiation (1486.6 eV).

2.5. Catalytic activity measurement

To evaluate the catalytic activity, the photodegradation of dye pollutants (RhB and methylene blue, 1×10^{-5} M) was conducted in the presence of Fe_3O_4@C@F-TiO_2 catalysts (0.2 g/L) under the visible-light ($\lambda > 420$ nm) from a 350 W Xe lamp equipped with a cutoff filter. Before light was turned on, the solution was stirred for 30 min in the dark to establish an adsorption–desorption equilibrium. The concentration of dye pollutants was monitored by real time detection on a UV/vis spectrometer. To study the stability of the Fe_3O_4@C@F-TiO_2 catalysts, repeat experiments on RhB decomposition were conducted under irradiation by visible-light. After each cycle, the Fe_3O_4@C@F-TiO_2 microspheres were separated from the solution with the aid of an external magnetic field and washed with ethanol and water. Then they were redispersed in a fresh dye solution for another cycle.

3. Results and discussion

The morphology and structure of the as-prepared samples were investigated by TEM. As presented in Fig. 1a, the Fe_3O_4@C microspheres show a core–shell structure in which the black Fe_3O_4 particles are encapsulated into thin gray carbon shells *ca.* 12 nm in thickness. As a result of carbonization of glucose, this uniform carbonaceous shell is proved to possess plenty of hydrophilic groups by FTIR spectroscopy. In Fig. S2a, the absorption peaks at 1702 cm^{-1} and 1616 cm^{-1} are assigned to C=O and C=C vibration, respectively, and the bands at 1000–1300 cm^{-1} are attributed to the C—OH stretching and O—H bending vibrations [32]. These results indicate the presence of plentiful hydrophilic functional groups on the carbon shell. The hydrophilic groups can not only improve the aqueous dispersibility of Fe_3O_4@C microspheres but also greatly enhance the affinity between the microspheres and Ti species [33]. Fig. 1b and c shows that the uniform Fe_3O_4@C@F-TiO_2 particles with an average diameter of 221 nm are obtained by solvothermal treating Fe_3O_4@C microspheres with TBT and HF in an ethanol solution. And from Fig. 1c, numerous TiO_2 nanoparticles can be clearly seen on the carbon surface forming a black layer. Compared with Fe_3O_4@C microspheres, the Fe_3O_4@C@F-TiO_2 microspheres possess a rough surface and the Fe_3O_4 cores are partly dissolved by HF transforming the structure from core–shell to yolk–shell. These two features may achieve a high surface area and be beneficial to improving catalytic performance. Without the addition of HF, the microspheres (Fe_3O_4@C@TiO_2) are also prepared and show an expected solid sandwich structure without the hollow inside the carbon shell (Fig. S3). The high-resolution TEM (HRTEM) images taken from the core and the shell of the Fe_3O_4@C@F-TiO_2 microspheres, as shown in Fig. 1d and e, respectively, confirm that the Fe_3O_4 core and the TiO_2 shell are well crystallized. The lattice spacing of 0.295 nm corresponds to the (2 2 0) plane of Fe_3O_4 [34], and the *d*-spacing of 0.353 nm matches to the d_{101} of anatase TiO_2 [35]. EDX analysis indicates the Fe_3O_4@C@F-TiO_2 microspheres are mainly composed of C, O, F, Ti and Fe, confirming the formation of fluorinated TiO_2 on the Fe_3O_4@C microspheres. The selected-area electron diffraction (SEAD) pattern (Fig. 1g) exhibits polycrystalline rings corresponding to the (1 0 1) and (4 0 0) planes of anatase TiO_2 and the (2 0 0) and (3 1 1) planes of Fe_3O_4.

High-angle annular dark-field scanning transmission electron microscopy (HAADF-STEM) imaging and EDX mapping further reveal the yolk–shell structure of the Fe_3O_4@C@F-TiO_2 microspheres with enhanced image contrast (Fig. 2). The Fe_3O_4 core is surrounded by the carbon layer supporting a hollow structure and the TiO_2 shell is outside the Fe_3O_4@C microsphere. It is noticeable that a small amount of F is detected in the region covering the TiO_2 shell, confirming the TiO_2 is successfully fluorinated. At the same time, on the Fe_3O_4 core the F element distribution is also observed. This may be ascribed to the sparingly soluble iron–fluoride complex formed during the etching process and subsequently absorbed on the Fe_3O_4 core [36,37].

To evaluate the interaction between carbon layer and TiO_2 shell, the Fe_3O_4@C@F-TiO_2 microspheres were examined by FTIR (Fig. S2b). Compared with the peaks of Fe_3O_4@C, the peaks for Fe_3O_4@C@F-TiO_2, belonging to the hydrophilic functional groups of the carbon layer as mentioned above, are significantly weakened ascribing to the TiO_2 nanoparticles growing on the carbon surface. In particular, the peak intensity ration of C=O vibration (1702 cm^{-1}) to C=C vibration (1616 cm^{-1}) changes from 1.16 to 0.62 after TiO_2 deposition, which may be related to the formation of C—O—Ti from C=O, suggesting a strong interaction at the interface of carbon and TiO_2 [5]. Fig. S4 depicts a TEM image of Fe_3O_4@F-TiO_2 microspheres prepared using the bare Fe_3O_4 as the template instead of the Fe_3O_4@C. It is apparent that only a few of Fe_3O_4 particles are successfully coated by TiO_2. This result demonstrates that the carbonaceous coating is crucial for TiO_2 deposition and implies that the existence of the interaction between carbon layer and TiO_2 shell. In addition, due to the decrease of crystallinity of Fe_3O_4 after being etched with HF, the characteristic band at 572 cm^{-1} for Fe_3O_4 becomes broad (Fig. S2b) [38].

The crystal structure and composition of Fe_3O_4@C@F-TiO_2 microspheres were identified by XRD, and for a comparison, the XRD pattern of Fe_3O_4@C@TiO_2 was also analyzed. In Fig. 3, both patterns indicate the anatase TiO_2 are formed on Fe_3O_4@C microspheres after solvothermal treatment. However, obviously, with HF added, TiO_2 possesses a stronger crystallization. This phenomenon is in good agreement with previous report that fluoride can enhance the crystallization of anatase phase and promotes the growth of crystallites owing to the rapid *in situ* fluoride-mediated dissolution–recrystallization (Eqs. (1) and (2)) [39].

$$4H^+ + TiO_2 + 6F^- \rightarrow TiF_6^{2-} + 2H_2O \quad \text{(dissolution)} \tag{1}$$

$$TiF_6^{2-} + 2H_2O \rightarrow 4H^+ + TiO_2 + 6F^- \quad \text{(recrystallization)} \tag{2}$$

By using the Scherrer equation, the average size of F-TiO_2 nanocrystals calculated from the full width at half maximum of the (1 0 1) peak is 7.2 nm, well consistent with the TEM result. Additionally, from the patterns no diffraction peak for the carbon is observed. It suggests the carbonaceous coating outside Fe_3O_4 particles is amorphous. The thermogravimetric analysis (TGA) results reveal the content of carbon in the Fe_3O_4@C@F-TiO_2 microspheres is as high as 40 wt% (Fig. S5).

To further confirm the chemical states of F in Fe_3O_4@C@F-TiO_2 microspheres, the XPS technique was employed. Fig. 4a shows the survey spectrum of Fe_3O_4@C@F-TiO_2 microspheres, from which the peaks of C, O, F and Ti elements with atomic concentrations of 53.94, 32.19, 2.92 and 10.95%, respectively, are observed. Since XPS is a surface analysis technique with investigation depth of 2–5 nm and the Fe_3O_4 cores are coated by carbon and TiO_2, the signal of Fe element is not detected. In Fig. 4b, the highly resolved XPS spectrum of F1s shows a single peak at 684.32 eV, which indicates the formation of surface fluoride (≡Ti—F) by ligand exchange between F^- and surface hydroxyl group on TiO_2 [17,40]. And the absence of signal at 688.50 eV suggests no F ions are incorporated into the TiO_2 lattice [41]. The Ti2p spectrum in Fig. S6a displays two peaks at 458.90 and 464.64 eV corresponding to the binding energies for $Ti2p_{3/2}$ and $Ti2p_{1/2}$, respectively. These results are in good agreement with the values in TiO_2 [42,43]. The C1s spectrum (Fig. S6b) is fitted to

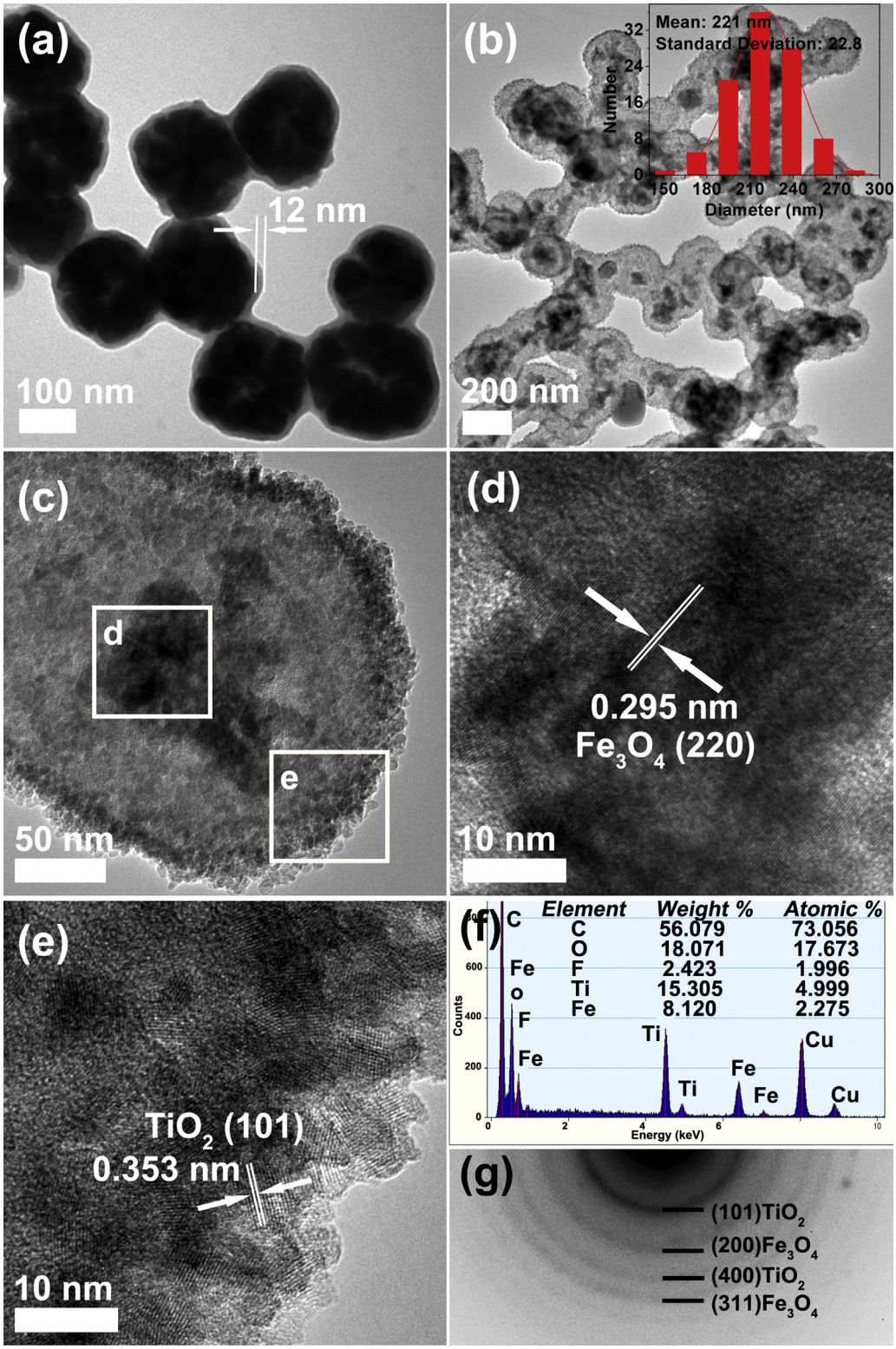

Fig. 1. TEM images of (a) Fe_3O_4@C and (b and c) Fe_3O_4@C@F-TiO_2 microspheres. (d and e) HRTEM images of the corresponding rectangular region in (c). (f) TEM-EDS analysis data and (g) SAED pattern of Fe_3O_4@C@F-TiO_2 microspheres. The Cu signal in (f) is detected from the Cu grid for TEM observation. The inset is diameter histogram of Fe_3O_4@C@F-TiO_2 microspheres and it is plotted based on >100 microspheres.

three peaks. The binding energies at 284.79, 286.00 and 288.97 eV can be assigned to C—C, C—O and COO bonds, respectively [44], providing another evidence for the existence of functional groups on carbon shell surface. In the O1s spectrum (Fig. S6c), the main fitting peak located at 530.06 eV is attributable to Ti—O bonding in TiO_2 [7,43], and the peaks at 531.37 and 533.02 eV are from C—O and O—H, respectively [45,46]. Obviously, all of these XPS results demonstrate that the Fe_3O_4@C@F-TiO_2 microspheres with surface fluorinated are successfully prepared. The optical absorption properties of Fe_3O_4@C@F-TiO_2 microspheres were investigated as displayed in Fig. S7. In comparison with the Fe_3O_4@C@TiO_2 microspheres, the Fe_3O_4@C@F-TiO_2 microspheres show a slight increase

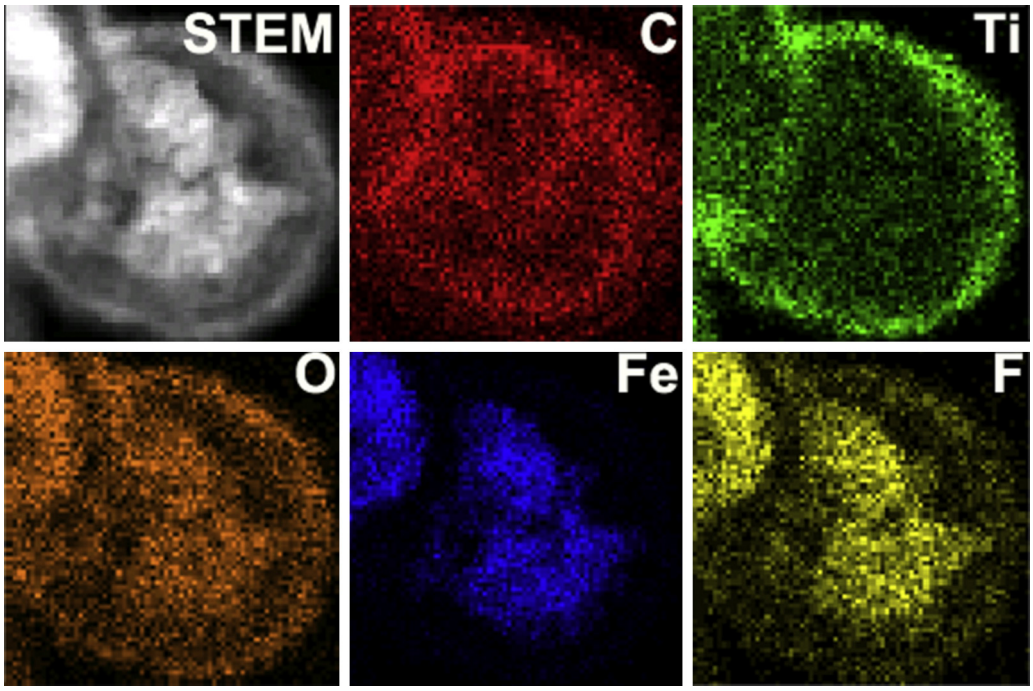

Fig. 2. HADDF-STEM image of a single Fe_3O_4@C@F-TiO_2 microsphere and corresponding EDS mapping images.

in absorption at $\lambda < 500$ nm, while the absorption edge is not modified by surface fluorination. This result is consistent with previous report and further confirms that the F element is not introduced into the TiO_2 lattice [47].

The magnetic property of the Fe_3O_4@C and Fe_3O_4@C@F-TiO_2 microspheres was quantified by using a superconducting quantum interference device magnetometer at 300 K. The hysteresis loops is illustrated in Fig. 5, which indicates that both samples show negligible coercivity and remanence. The saturation magnetization (M_s) for Fe_3O_4@C is about 18.3 emu/g, and that of Fe_3O_4@C@F-TiO_2 is about 2.6 emu/g. The great decrease in M_s could be attributed to the introduction of nonmagnetic TiO_2 shell, which quenches the magnetic moment [48]. Another factor may be correlated to the synergistic effect of the structure distortions and mass decrease of the Fe_3O_4 core caused by etching of HF [49,50]. Even with the reduction in M_s, the yolk–shell Fe_3O_4@C@F-TiO_2 microspheres can still be efficiently separated from the solution with the aid of an external magnetic field. The N_2 adsorption–desorption isotherm of

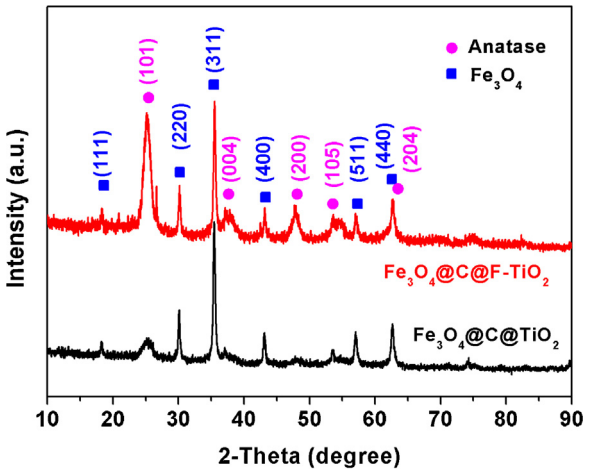

Fig. 3. XRD spectra of Fe_3O_4@C@F-TiO_2 and Fe_3O_4@C@TiO_2 microspheres.

Fe_3O_4@C@F-TiO_2 microspheres exhibits a typical type IV isotherm with a type H3 hysteresis loop, characteristic of mesoporous materials with the hollow interior (Fig. 6) [51]. The BET surface area and total pore volume are calculated to be 167.50 m^2/g (over two times that for large hollow TiO_2 microspheres reported by Jaroniec et al. [21]) and 0.207 cm^3/g, respectively. The desorption isotherm shows a major capillary condensation step at the relative pressure ranges of 0.4–0.6 and a minor step at 0.6–0.85. By using Barrett–Joyner–Halenda model, these two steps correspond to two distinct peaks at 3.7 and 4.2 nm, respectively, in the pore size distribution curve (inset of Fig. 6) [52]. The N_2 adsorption isotherm of Fe_3O_4@C@TiO_2 microspheres is also displayed in Fig. S8, which shows a much smaller BET surface area of 49.46 m^2/g than that of Fe_3O_4@C@F-TiO_2. Meanwhile, combined with the TEM observation, the disappearance of H3 hysteresis loop further provides evidence of the absence of hollow interior inside the Fe_3O_4@C@TiO_2 microspheres. These results indicate the addition of HF does cause the yolk–shell structure formation and greatly increase the surface area of the Fe_3O_4@C@F-TiO_2 microspheres.

Due to the magnetic separability and the high surface area, the yolk–shell structured Fe_3O_4@C@F-TiO_2 microspheres with surface fluorinated are expected to be ideal candidates for catalytic application. The photocatalytic performance of Fe_3O_4@C@F-TiO_2 microspheres was tested by degradation of RhB and methylene blue under visible-light irradiation. In Fig. 7a, in the presence of Fe_3O_4@C@F-TiO_2 microspheres, the RhB is completely degraded after irradiation for 80 min under visible-light. However, when the suspension is stirred in dark or irradiated with visible-light in the absence of catalysts, there is no obvious degradation of RhB detected (Fig. 7b). These results indicate that it is the as-prepared Fe_3O_4@C@F-TiO_2 microspheres that utilize the visible-light to degrade the RhB molecules. Furthermore, the Degussa P25 TiO_2 (surface area of 52.53 m^2/g)[53] and the Fe_3O_4@C@TiO_2 microspheres (surface area of 49.46 m^2/g) are used as references for comparison. As shown in Fig. 7b, the Fe_3O_4@C@F-TiO_2 microspheres exhibit the highest photocatalytic activity for degradation of RhB over the P25 TiO_2 powders and the Fe_3O_4@C@TiO_2 microspheres. According to the method reported previously, the

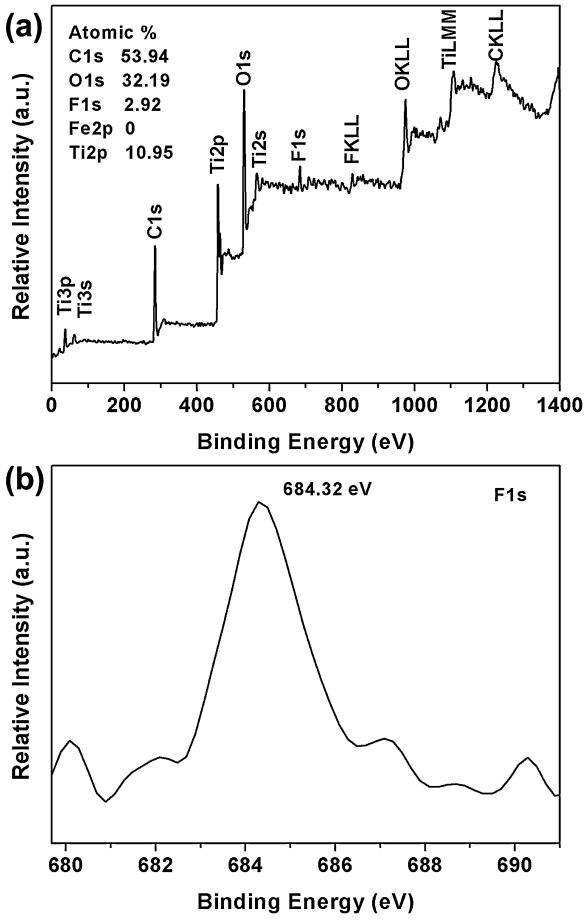

Fig. 4. XPS spectra of Fe_3O_4@C@F-TiO_2 microspheres: (a) survey and (b) F1s.

degradation data is fitted and shows pseudo-first order reaction kinetics (Fig. S10) [10,54]. The apparent rate constant k for Fe_3O_4@C@F-TiO_2 microspheres is calculated as 0.038 min^{-1}, which is about 2.00 and 6.33 times that for Fe_3O_4@C@TiO_2 and P25 TiO_2, respectively. The excellent catalytic performance of the Fe_3O_4@C@F-TiO_2 microspheres may be attributed to the yolk–shell structure with high surface area, the good dispersibility and the synergic effect of carbon modification and surface fluorination for TiO_2. The high surface area and the good dispersibility are

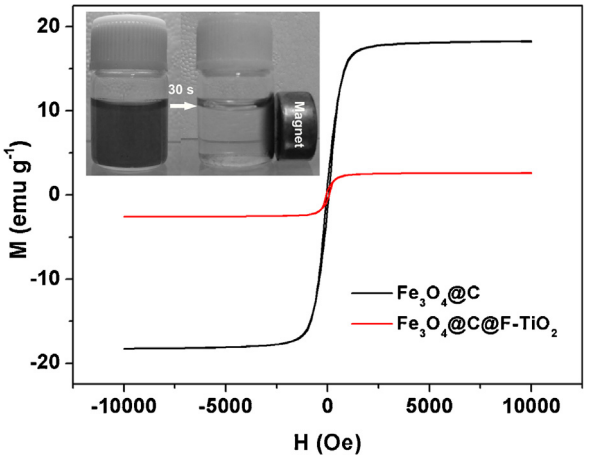

Fig. 5. Room temperature field-dependent magnetization curves of Fe_3O_4@C and Fe_3O_4@C@F-TiO_2 microspheres. The inset shows the Fe_3O_4@C@F-TiO_2 microspheres suspended in water are attracted to the walls of the vial when a magnet is present for 30 s.

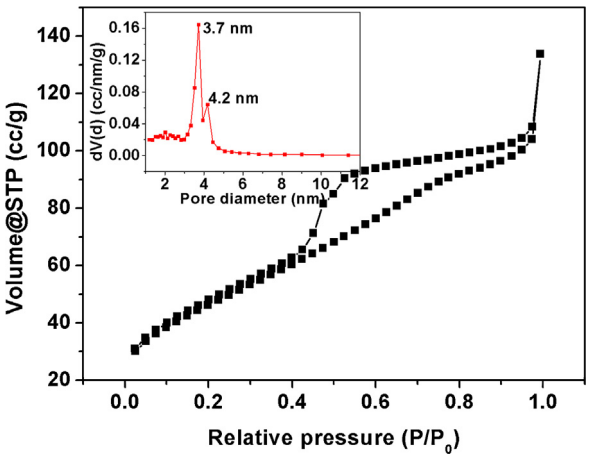

Fig. 6. N_2 adsorption–desorption isotherm of Fe_3O_4@C@F-TiO_2 microspheres. Inset shows the pore size distribution driven from the desorption branch.

beneficial for transportation and adsorption of RhB molecules and can provide more reaction sites for degradation of RhB, thus promoting the catalytic reaction [55]. At the same time, the TiO_2 shell has been proved to have a strong interaction and good contact with carbon mid-layer by the FTIR spectra (Fig. S2b). Therefore, the carbon mid-layer with an excellent electronic conductivity could be used as the electron acceptor and transporter to suppress the carriers (holes and electrons) recombination, leading to improved photocatalytic efficiency [27,56,57]. The carrier separation principle between carbon and TiO_2 is illustrated in Fig. S11. Additionally, after the surface fluorination, the TiO_2 possesses a good crystallization with small crystallite size. Moreover, the ≡Ti—F group can act as an electron-trapping site to trap the photogenerated electrons due to the strong electronegativity of the fluorine, resulting in the reduction of the recombination rate of electron and hole and enhancement of photocatalytic activity [40]. Meanwhile, the high photocatalytic efficiency of Fe_3O_4@C@F-TiO_2 microspheres can also attribute to that more mobile free OH radicals could be generated on F-TiO_2 than those on naked TiO_2 (Eqs. (3) and (4)) [40,58,59].

$$\equiv Ti{-}F + H_2O_{ads} \quad (\text{or } OH^-) + h_{vb}{}^+ \rightarrow \equiv Ti{-}F + {}^{\bullet}OH_{free} + H^+ \qquad (3)$$

$$\equiv Ti{-}OH + h_{vb}{}^+ \rightarrow \equiv Ti{-}{}^{\bullet}OH_{ads}{}^+ \qquad (4)$$

According to the Langmuir–Hinshelwood mechanism, before the species begin to degrade, the adsorption of species is required in the photocatalytic degradation process [18]. It means a higher adsorption of species yields higher photocatalytic activity. The surface of fluorinated TiO_2 is negatively charged and possesses the high adsorption capacity for cationic dyes (RhB, methylene blue, *etc.*) because of electrostatic attract [3,60]. Thus a high photocatalytic activity could be achieved.

The stability and repeatability of the catalyst are of great significance for practical application, so the cycling experiments on RhB degradation over the Fe_3O_4@C@F-TiO_2 microspheres were conducted. As shown in Fig. 7c, the Fe_3O_4@C@F-TiO_2 microspheres exhibit stable degradation efficiency after four cycles. Interestingly, the degradation rate during the first cycle is relative small but increases fast in following cycles. This result is well consistent with the previous report by Kuang et al. and could be due to the desorption of inorganic species from the TiO_2 surface and the degradation of organic adsorbates on the surface after the first cycle [10]. When the Fe_3O_4@C@F-TiO_2 microspheres were cleaned with 0.1 M NaOH to remove the inorganic species and the organic adsorbates, the degradation efficiency of the catalyst still shows no improvement (Fig. S12). This phenomenon is different from the result reported

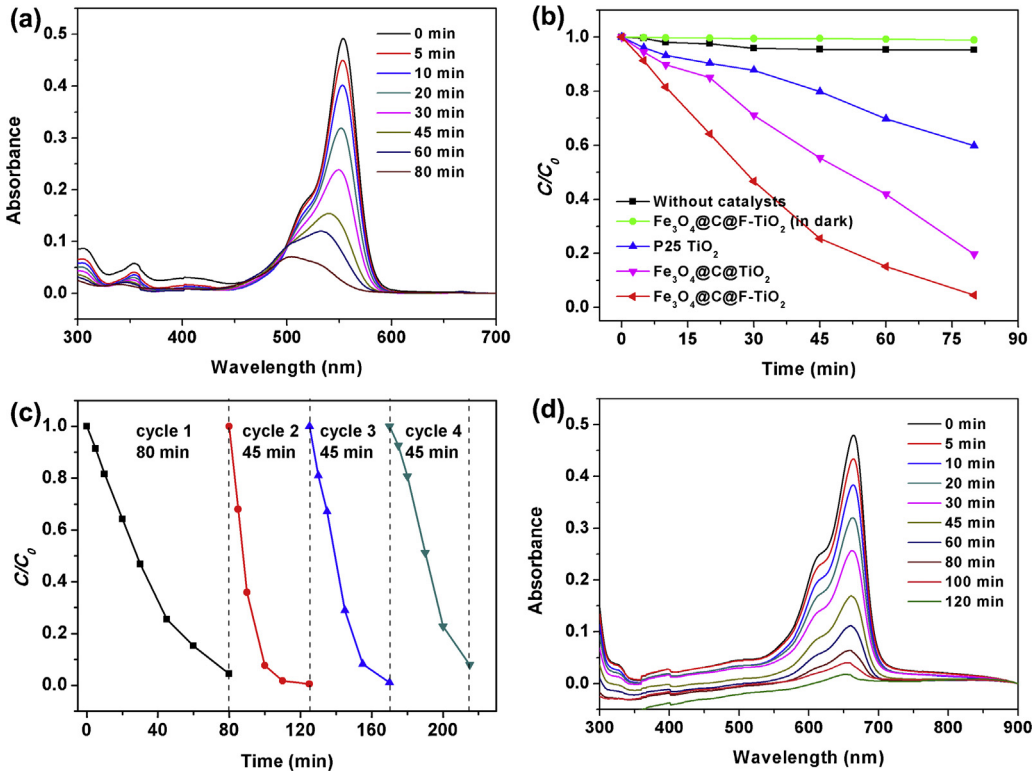

Fig. 7. Time-dependent absorption spectra of (a) RhB and (d) methylene blue solution in the presence of Fe_3O_4@C@F-TiO_2 microspheres. (b) Comparison of data for catalytic degradation of RhB over different catalysts under visible-light irradiation (without any catalyst – squares; Fe_3O_4@C@F-TiO_2 in dark – diamonds; P25 TiO_2 – triangles; Fe_3O_4@C@TiO_2 – inverted triangles; Fe_3O_4@C@F-TiO_2 – left triangles). (c) Cycling degradation of RhB with Fe_3O_4@C@F-TiO_2 microspheres.

by Kuang et al. and could be explained as follows. Cleaning with alkaline solution can remove the inorganic and organic adsorbates, which certainly promote the photocatalytic process. However, it also can replace the ≡Ti—F with ≡Ti—OH by a ligand exchange reaction between OH^- in the NaOH solution and F^- on TiO_2 [61], which reduces the adsorption capacity of photocatalysts to RhB and causes more recombination of photogenerated holes and electrons, resulting in the reduction of degradation efficiency. In the present case, the catalytic process may be dominated by the latter effect. Thus the degradation efficiency is hardly improved. As for the cycling experiments, since the catalytic reaction is performed in neutral solution and the ligand exchange reaction between OH^- and F^- is negligible, the degradation rate is accelerated by the former factor. The as-prepared Fe_3O_4@C@F-TiO_2 microspheres were also used for decomposing methylene blue under visible-light irradiation. On irradiation for 120 min, almost 100% of methylene blue molecules are decomposed. This result further indicates the yolk–shell structured Fe_3O_4@C@F-TiO_2 microspheres possess an excellent visible-light driven catalytic activity.

4. Conclusions

In conclusion, a novel kind of yolk–shell structured Fe_3O_4@C@F-TiO_2 microspheres with carbon modified and surface fluorinated anatase outer-shell have been prepared by a template-based solvothermal etching method with the assistance of HF. The HF used here enhances the growth of anatase crystallites with surface fluorinated and leads to the yolk–shell structure formation though partly etching Fe_3O_4 cores. The presence of magnetic Fe_3O_4 cores makes the Fe_3O_4@C@F-TiO_2 microspheres highly reproducible. Due to the large surface area, good dispersibility, carbon modification and plenty of ≡Ti—F groups on TiO_2 surface, the Fe_3O_4@C@F-TiO_2 microspheres show a higher visible-light driven photocatalytic activity for RhB degradation than P25 TiO_2 and the Fe_3O_4@C@TiO_2 microspheres. The ≡Ti—F groups on TiO_2 surface not only as electron-trapping sites can reduce the recombination of photogenerated electrons and holes but also can enhance the adsorption capacity for RhB. More importantly, the catalytic activity of Fe_3O_4@C@F-TiO_2 microspheres is stable. These features might offer the Fe_3O_4@C@F-TiO_2 microspheres new opportunities for practical application as catalysts.

Acknowledgements

This work was financially supported by the National Natural Science Foundation of China (Grant Nos. 50802061 and 51372169) and Natural Science Foundation of Tianjin (Grant No. 11JCZDJC17300).

Appendix A. Supplementary data

Supplementary material related to this article can be found, in the online version, at http://dx.doi.org/10.1016/j.apcatb.2013.12.050.

References

[1] Z. Yi, J. Ye, N. Kikugawa, T. Kako, S. Ouyang, H. Stuart-Williams, H. Yang, J. Cao, W. Luo, Z. Li, Nat. Mater. 9 (2010) 559–564.
[2] A. Fujishima, K. Honda, Nature 238 (1972) 37–38.
[3] J. Tang, H. Quan, J. Ye, Chem. Mater. 19 (2007) 116–122.
[4] X. Chen, C. Burda, J. Am. Chem. Soc. 130 (2008) 5018–5019.
[5] D. Sun, J. Yang, X. Wang, Nanoscale 2 (2010) 287–292.
[6] Z. Xiong, X.S. Zhao, J. Am. Chem. Soc. 134 (2012) 5754–5757.
[7] X. Li, F. He, G. Liu, Y. Huang, C. Pan, C. Guo, Mater. Lett. 67 (2012) 369–372.
[8] C. Ratanatawanate, C. Xiong, K.J. Balkus, ACS Nano 2 (2008) 1682–1688.
[9] C. Cheng, S.K. Karuturi, L. Liu, J. Liu, H. Li, L.T. Su, A.I.Y. Tok, H.J. Fan, Small 8 (2012) 36.
[10] X. Han, Q. Kuang, M. Jin, Z. Xie, L. Zheng, J. Am. Chem. Soc. 131 (2009) 3152–3153.

[11] Q. Xiang, K. Lv, J. Yu, Appl. Catal., B 96 (2010) 557–564.
[12] Q. Zhang, D.Q. Lima, I. Lee, F. Zaera, M. Chi, Y. Yin, Angew. Chem. Int. Ed. 123 (2011) 7226–7230.
[13] C. Zhang, F. Liu, Y. Zhai, H. Ariga, N. Yi, Y. Liu, K. Asakura, M. Flytzani-Stephanopoulos, H. He, Angew. Chem. Int. Ed. 51 (2012) 9628–9632.
[14] R. Su, R. Tiruvalam, Q. He, N. Dimitratos, L. Kesavan, C. Hammond, J.A. Lopez-Sanchez, R. Bechstein, C.J. Kiely, G.J. Hutchings, ACS Nano 6 (2012) 6284–6292.
[15] F. Xiao, Chem. Commun. (2012) 6538–6540.
[16] S. Liu, J. Yu, B. Cheng, M. Jaroniec, Adv. Colloid Interface Sci. 173 (2012) 35–53.
[17] C.Y. Jimmy, J. Yu, W. Ho, Z. Jiang, L. Zhang, Chem. Mater. 14 (2002) 3808–3816.
[18] K. Woan, G. Pyrgiotakis, W. Sigmund, Adv. Mater. 21 (2009) 2233–2239.
[19] H. Pan, J. Qian, Y. Cui, H. Xie, X. Zhou, J. Mater. Chem. 22 (2012) 6002–6009.
[20] J.H. Pan, X. Zhang, A.J. Du, D.D. Sun, J.O. Leckie, J. Am. Chem. Soc. 130 (2008) 11256–11257.
[21] H.H. Wang, F. Tian, X.P. Li, F.L. Liu, Q. Shen, Powder Technol. 197 (2010) 298–302.
[22] L. Junqi, W. Defang, L. Hui, H. Zuoli, Z. Zhenfeng, Appl. Surf. Sci. 257 (2011) 5879–5884.
[23] J. Yu, S. Liu, H. Yu, J. Catal. 249 (2007) 59–66.
[24] M. Liu, K.L. Lv, G.H. Wang, Z.Y. Wang, Y.X. Zhao, Y.R. Deng, Chem. Eng. Technol. 33 (2010) 1531–1536.
[25] Y.H. Ng, S. Ikeda, M. Matsumura, R. Amal, Energy Environ. Sci. 5 (2012) 9307–9318.
[26] J. Hou, S. Jiao, H. Zhu, R.V. Kumar, CrystEngComm 13 (2011) 4735–4740.
[27] H. Zhang, X. Lv, Y. Li, Y. Wang, J. Li, ACS Nano 4 (2009) 380–386.
[28] F. Shi, Y. Li, Q. Zhang, H. Wang, Int. J. Photoenergy 2012 (2012).
[29] M. Ye, Q. Zhang, Y. Hu, J. Ge, Z. Lu, L. He, Z. Chen, Y. Yin, Chem. Eur. J. 16 (2010) 6243–6250.
[30] S. Xuan, Y.-X.J. Wang, J.C. Yu, K.C.-F. Leung, Langmuir 25 (2009) 11835–11843.
[31] J. Bao, W. Chen, T. Liu, Y. Zhu, P. Jin, L. Wang, J. Liu, Y. Wei, Y. Li, ACS Nano 1 (2007) 293–298.
[32] X. Sun, Y. Li, Angew. Chem. Int. Ed. 43 (2004) 597–601.
[33] D. Qi, J. Lu, C. Deng, X. Zhang, J. Phys. Chem. C 113 (2009) 15854–15861.
[34] C. Wang, Y. Wei, H. Jiang, S. Sun, Nano Lett. 9 (2009) 4544–4547.
[35] Y. Dai, C.M. Cobley, J. Zeng, Y. Sun, Y. Xia, Nano Lett. 9 (2009) 2455–2459.
[36] A.V. Pomosov, I.B. Murashova, V.P. Artamonov, Powder Metall. Met. Ceram. 8 (1969) 341–344.
[37] D. Suter, S. Banwart, W. Stumm, Langmuir 7 (1991) 809–813.
[38] G. Xie, P. Xi, H. Liu, F. Chen, L. Huang, Y. Shi, F. Hou, Z. Zeng, C. Shao, J. Wang, J. Mater. Chem. 22 (2012) 1033–1039.
[39] Z. Wang, K. Lv, G. Wang, K. Deng, D. Tang, Appl. Catal., B 100 (2010) 378–385.
[40] H. Park, W. Choi, J. Phys. Chem. B 108 (2004) 4086–4093.
[41] J. Zhu, D. Zhang, Z. Bian, G. Li, Y. Huo, Y. Lu, H. Li, Chem. Commun. (2009) 5394–5396.
[42] X. Sun, M. Xie, G. Wang, H. Sun, A.S. Cavanagh, J.J. Travis, S.M. George, J. Lian, J. Electrochem. Soc. 159 (2012) A364–A369.
[43] B.-S. Huang, H.-H. Tseng, M.-Y. Wey, J. Ceram. Soc. Jpn. 117 (2009) 753–758.
[44] G. An, W. Ma, Z. Sun, Z. Liu, B. Han, S. Miao, Z. Miao, K. Ding, Carbon 45 (2007) 1795–1801.
[45] X.-b. Yan, B.K. Tay, Y. Yang, J. Phys. Chem. B 110 (2006) 25844–25849.
[46] H.-T. Fang, C.-G. Liu, C. Liu, F. Li, M. Liu, H.-M. Cheng, Chem. Mater. 16 (2004) 5744–5750.
[47] J. Yu, W. Wang, B. Cheng, B.L. Su, J. Phys. Chem. C 113 (2009) 6743–6750.
[48] H. Wang, L. Sun, Y. Li, X. Fei, M. Sun, C. Zhang, Q. Yang, Langmuir 27 (2011) 11609–11615.
[49] R.H. Kodama, A.E. Berkowitz, J.E.J. McNiff, S. Foner, J. Appl. Phys. 81 (1997) 5552–5557.
[50] A. Punnoose, H. Magnone, M.S. Seehra, J. Bonevich, Phys. Rev. B 64 (2001) 174420–174427.
[51] Y. Yang, J. Liu, X. Li, X. Liu, Q. Yang, Chem. Mater. 23 (2011) 3676–3684.
[52] T. Zhang, Q. Zhang, J. Ge, J. Goebl, M. Sun, Y. Yan, Y. Liu, C. Chang, J. Guo, Y. Yin, J. Phys. Chem. C 113 (2009) 3168–3175.
[53] G. Liu, F. He, X. Li, S. Wang, L. Li, G. Zuo, Y. Huang, Y. Wan, J. Mater. Chem. 21 (2011) 10637–10640.
[54] X. Shen, L. Zhu, C. Huang, H. Tang, Z. Yu, F. Deng, J. Mater. Chem. 19 (2009) 4843–4851.
[55] W. Li, Y. Deng, Z. Wu, X. Qian, J. Yang, Y. Wang, D. Gu, F. Zhang, B. Tu, D. Zhao, J. Am. Chem. Soc. 133 (2011) 15830–15833.
[56] X.H. Huang, J.P. Tu, C.Q. Zhang, X.T. Chen, Y.F. Yuan, H.M. Wu, Electrochim. Acta 52 (2007) 4177–4181.
[57] Y. Liu, M. Zhou, Y. Hu, H. Qian, J. Chen, X. Hu, CrystEngComm 14 (2012) 4507–4512.
[58] C. Minero, G. Mariella, V. Maurino, E. Pelizzetti, Langmuir 16 (2000) 2632–2641.
[59] C. Minero, G. Mariella, V. Maurino, D. Vione, E. Pelizzetti, Langmuir 16 (2000) 8964–8972.
[60] Q. Wang, C. Chen, D. Zhao, W. Ma, J. Zhao, Langmuir 24 (2008) 7338–7345.
[61] H.G. Yang, C.H. Sun, S.Z. Qiao, J. Zou, G. Liu, S.C. Smith, H.M. Cheng, G.Q. Lu, Nature 453 (2008) 638–641.